

Modelling and identification of the da Vinci Research Kit robotic arms

G. A. Fontanelli, F. Ficuciello, L. Villani, B. Siciliano

Abstract—The da Vinci Research Kit (DVRK) is a telerobotic surgical research platform endowed with an open controller that allows position, velocity and current control. We consider the problem of modelling and identification of both the Patient Side Manipulators (PSMs) and of the Master Tool Manipulators (MTMs) of the platform. This problem is relevant when realistic dynamic simulations have to be performed using standard software tools, but also for the design of model-based control laws, and for the implementation of sensorless strategies for collision detection or contact force estimation. A LMI-based approach is used for the identification of the robot dynamics in order to guarantee the physical feasibility of the parameters that is not ensured by standard least-squares methods. The identified models are validated experimentally.

I. INTRODUCTION

The da Vinci Research Kit (DVRK) is a telerobotic surgical research platform assembled using a collection of robotic components from the first-generation da Vinci Surgical System provided by Intuitive Surgical. The DVRK is currently used by 26 research groups around the world [1]. The platform (see Fig. 1) consists of two patient side manipulators (PSMs), one endoscopic manipulator and two master tool manipulators (MTMs). An open controller developed by the John Hopkins University [2] provides a full ROS-based control of all the DVRK robotic arms. The controller allows position, velocity and current control and thus opens the way for developing and testing advanced control techniques, like impedance control, force control and bilateral tele-manipulation control.

Complete and accurate dynamic models of the DVRK robotic arms are necessary in order to design model-based control laws, but also for realistic dynamic simulations and to implement sensorless strategies for collision detection or contact force estimation [3], [4], [5] in lieu of direct sensing [6]. These latter can be conveniently employed to improve surgeons perception and ability.

The aim of this work is to derive a complete dynamic model of both the MTMs and the PSMs arms of the DVRK system and use state of the art methods to obtain accurate identification of the dynamic parameters.

The identification of the dynamic model of a robot is usually addressed using linear regression techniques based on the linear dependence of the dynamic equations with respect to a set of dynamic coefficients, also known as base parameters [7].

The obtained results are not necessarily physically consistent [8], and may generate problems in simulation or control. A number of approaches have been developed to

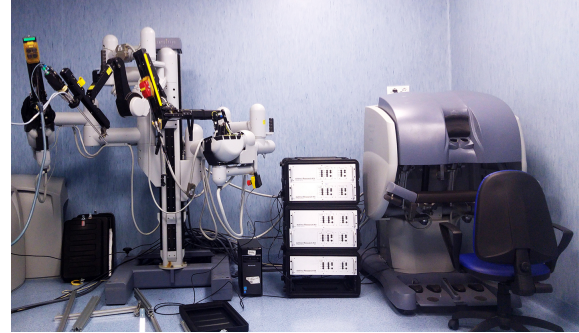


Fig. 1. The da Vinci Research Kit available at ICAROS center

ensure physical consistency (see, e.g., [9], [10]); some of them allow to formulate the constraints as Linear Matrix Inequalities (LMIs) and guarantee global optimality of the solution through semidefinite programming [11].

To the best of our knowledge, this is the first paper dealing with accurate dynamic modelling and identification of the DVRK robotic arms. The modelling is complicated for the presence of a 1-DOF double parallelogram and a counterweight in the PSM, and of a 2-DOF parallelogram in the MTM. Moreover, all the motors of the PSM are located at the base of the robot and the joints are driven through cables introducing elasticity, backlash and non-linear friction, which are difficult to model. A constrained optimisation approach based on LMIs has been adopted to guarantee physical consistency of the dynamic parameters. The results of the experimental validation of the identified models are satisfactory, especially for the PSM, although they could be further improved.

II. DVRK KINEMATIC AND DYNAMIC MODELLING

In this section the procedure to derive the kinematic and dynamic model of both the PSM and MTM are presented.

A. PSM arm kinematics

Each PSM is a 7-DOF actuated arm, which moves a surgical instrument about a Remote Center of Motion (RCM), i.e., a fixed fulcrum point that is invariant to the configuration of the PSM joints [12].

In detail, with reference to Fig. 2:

- the overall structure may rotate about axis J_1 of an angle θ_1 ;
- a double parallelogram mechanism allows the rotation of the surgical instrument about axis J_2 of an angle θ_2 ;
- the surgical instrument may translate along axis J_3 of a length d_3 and rotate about axis $J_4 \equiv J_3$ of an angle θ_4 ;
- the axes J_1 , J_2 , J_3 and J_4 intersect in the RCM, whose position does not depend on the joint variables;

The authors are with the Interdepartmental Center for Advances in Robotic Surgery of the University of Naples Federico II. Corresponding author's email: giuseppeandrea.fontanelli@unina.it

- the revolute joints J_5 (angle θ_5) and J_6 (angle θ_6) are orthogonal and, together with J_4 , form a non-spherical wrist.

The first 6 degrees of freedom correspond to Revolute (R) or Prismatic (P) joints, combined in a RRP RRR sequence. The last degree of freedom, corresponding to the opening and closing motion of the gripper, is not considered here since we are interested in computing the position and orientation of a frame attached to the center of the gripper (frame g) with respect to a base frame (frame b) as a function of the joint vector:

$$\mathbf{q} = [\theta_1 \quad \theta_2 \quad d_3 \quad \theta_4 \quad \theta_5 \quad \theta_6]^T.$$

The homogeneous transformation matrix $T_g^b(\mathbf{q})$, representing the pose of the gripper frame g with respect to the base frame b , can be easily computed by choosing the origin of frame b in the RCM point and applying the standard Denavit-Hartenberg (DH) convention [13] to the kinematic chain $\{J_1, \dots, J_6\}$ of Fig. 2.

Noticeably, for the computation of $T_g^b(\mathbf{q})$, the kinematics of the double parallelogram can be ignored. Moreover, the PSM arm is mounted on a passive base (the so-called setup joint) which allows translating and rotating the arm with respect to the patient, i.e., modifying the position and orientation of the frame b attached to the RCM. Hence, a suitable constant homogeneous transformation matrix T_b^w must be introduced to define the position and orientation of the base frame b with respect to a world frame w .

In computing the dynamic model of the PSM, the constant rotation R_b^w of the base frame b with respect to the world frame w must be taken explicitly into account because it affects the gravity torque reflected at the joints.

TABLE I
DH PARAMETERS OF THE PSM

link	joint	prev	succ	a_i	α_i	d_i	θ_i
1	R	—	2	0	$-\pi/2$	—	θ_1
2	R	1	2', χ	0.2	0	—	θ_2
2'	R	2	2''	0.5	0	—	$\theta_{2'}$
2''	R	2'	3	0	$-\pi/2$	—	$\theta_{2''}$
3	P	2''	4	0	0	d_3	—
4	R	3	5	0	$\pi/2$	—	θ_4
5	R	4	6	0.009	$-\pi/2$	—	θ_5
6	R	5	—	0	$-\pi/2$	—	θ_6
χ	P	2	c	0	$-\pi/2$	—	—
c	P	χ	—	0	0	d_c	—

B. PSM arm dynamics

The computation of the dynamic model of the PSM arm can be performed using, e.g., the recursive Newton-Euler approach [13]. The classical version of the algorithm for open kinematic chains must be suitably modified to include the dynamic effects of:

- the counterweight used to balance the motion of the instrument along the prismatic joint (see Fig. 3);
- the links of the double parallelogram mechanism.

With reference to Fig. 3, representing the complete kinematic structure of the PSM, the forward and backward

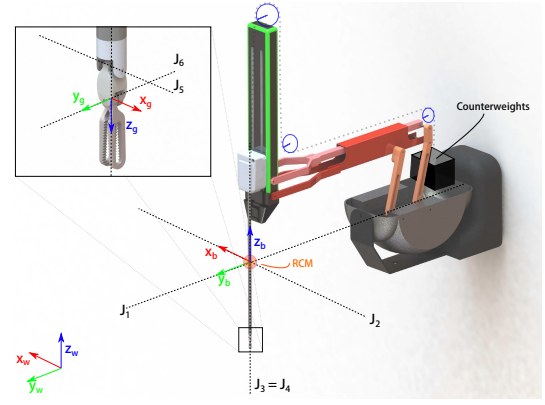


Fig. 2. Patient Side Manipulator (PSM) kinematics

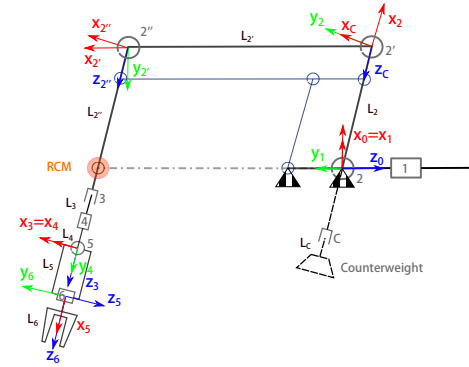


Fig. 3. Schematic of the PSM kinematics with the Denavit-Hartenberg frames

recursions can be applied to the open kinematic chain composed by joints $\{1, 2, 2', 2'', 3, 4, 5, 6\}$. An additional branch of the chain must be considered to take into account the counterweight. The effects of the double parallelogram can be accounted by imposing constraints to the kinematic variables and to the joint torques.

Table I reports the Denavit-Hartenberg parameters corresponding to the reference frames set as in Fig. 3, using the notation of the book [13]. In particular, the joint variable q_i is denoted as θ_i in case of revolute joint and as d_i in case of prismatic joint.

The last two rows of the table allows to take into account the counterweight, modelled as a link which slides along a prismatic joint attached to link L_2 and linked by a tendon driven mechanism to the actuator of the prismatic joint 3. In detail, row c specifies a frame attached to the counterweight, while row χ corresponds to a frame attached to a fictitious link L_χ , which coincides with link L_2 and must be introduced to comply with the Denavit-Hartenberg convention.

Thus the Newton-Euler algorithm, which is omitted here for brevity, allows computing the (6×1) vector of the joint torques τ taking into account the inertia, Coriolis, centrifugal and gravity generalised forces. The contributions due to joint friction and to elastic forces acting on some of the joints can be added separately, i.e.: $\tau_{PSM} = \tau + \tau_f + \tau_e$.

The friction contribution τ_f has been set as the sum of

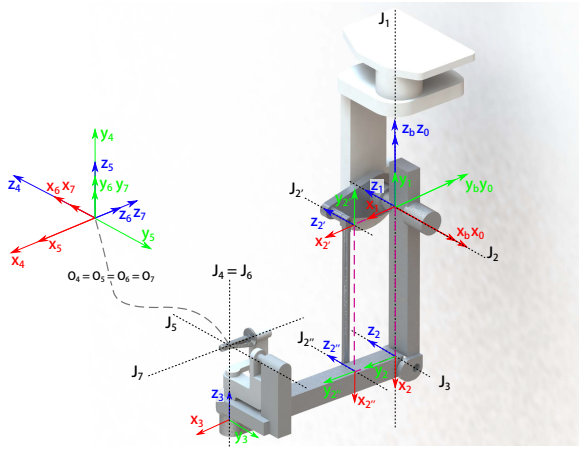


Fig. 4. Master tool Manipulator (MTM) kinematics with Denavit-Hartenberg frames

viscous and static friction:

$$\tau_f = F_v \dot{q} + F_s \text{sgn}(\dot{q}), \quad (1)$$

with $F_v = \text{diag}\{F_{v1}, \dots, F_{v4}, F_{vl}\}$, where F_{vl} is a (2×2) matrix and $F_s = \text{diag}\{F_{s1}, \dots, F_{s6}\}$. Matrix F_{vl} models the viscous friction for the last 2 joints, that are coupled by a tendon driving mechanism.

The elastic contribution τ_e models the elastic forces acting on some joints. In particular, for joint 1 and 2 the elasticity is created by the power cables, while an elastic torque produced by a torsional spring is present on joint 4. These torques tend to bring back the joints to their zero angular positions and can be modeled as:

$$\tau_e = K_e q, \quad (2)$$

with $K_e = \text{diag}\{K_{e1}, K_{e2}, 0, K_{e4}, 0, 0\}$. Finally, for the last three links, the mass and inertia properties have been neglected and the corresponding parameters have been set to zero.

C. MTM arm kinematics

The two MTMs, used to remotely teleoperate the two PSMs and the endoscopic manipulator, are identical except for their wrists, that are mirrored. Each MTM is an 8-DOF manipulator. The last degree of freedom is not actuated by a motor and is used to command the opening and closing of the gripper of the instrument. Only the first 7 degrees of freedom are considered in the kinematic and dynamic model described here.

In detail, with reference to Fig. 4:

- the overall structure may rotate about the vertical axis J_1 of an angle θ_1 ;
- the revolute joints with axes J_2 , J_2' , J_2'' and J_3 form a 2-DOF parallelogram mechanism; the two actuated joints of the parallelogram are those about axes J_2 (angle θ_2) and J_3 (angle θ_3);
- the axes J_4 , J_5 , J_6 and J_7 intersect in the same point and correspond to revolute joints with angles θ_4 , θ_5 , θ_6 and θ_7 .

All the joints are actuated by a motor, with the exception of the two revolute joints of the parallelogram about axes J_2' and J_2'' .

The kinematic model of the MTM arm can be computed as a function of the vector of the actuated joints: $q = [\theta_1 \dots \theta_7]^T$ by using the DH convention extended to closed kinematic chains [13]. The reference frames corresponding to the DH table reported in Table II are shown in Fig. 4. Note that the base frame b coincides with frame 0.

The homogenous transformation matrix $T_7^b(q)$ can be computed, e.g., by considering the kinematic chain $\{1, 2, 3, 4, 5, 6, 7\}$ and taking into account that the parallelogram mechanism imposes the following constraints to the joint variables:

$$q_{2'} = q_2 + q_3, \quad q_{2''} = -q_3. \quad (3)$$

TABLE II
DH PARAMETERS OF THE MTM

link	joint	prev	succ	a_i	α_i	d_i	θ_i
1	R	—	2, 2'	0	$\pi/2$	0	θ_1
2	R	1	3	0.279	0	0	θ_2
2'	R	1	2''	0.1	0	0	$\theta_{2'}$
2''	R	2'	—	0.279	0	0	$\theta_{2''}$
3	R	2	4	0.365	$-\pi/2$	0	θ_3
4	R	3	5	0	$\pi/2$	0.151	θ_4
5	R	4	6	0	$-\pi/2$	0	θ_5
6	R	5	7	0	$\pi/2$	0	θ_6
7	R	6	—	0	0	0	θ_7

D. MTM arm dynamics

The computation of the dynamic model of the MSM arm, as for the PSM arm, can be performed using the recursive Newton-Euler approach. The version of the algorithm for closed kinematic chains must be adopted, to take into account for the parallelogram mechanism.

The algorithm allows computing the (7×1) vector of the joint torques τ taking into account the inertia, Coriolis, centrifugal and gravity torques. The contributions due to joint friction and to elastic torques acting on some of the joints are added separately, i.e.: $\tau_{MTM} = \tau + \tau_f + \tau_e$. The friction contribution τ_f has been set as the sum of viscous and static friction as in (1) with F_s and F_v set as diagonal matrices. The torque τ_e , set as in (2) with diagonal K_e , models the elastic torques acting on joint 1, due to the power cables, and on joints 4, 5 and 6, caused by torsional springs.

III. IDENTIFICATION OF THE DYNAMIC PARAMETERS

The methods of identification of the dynamic model of a rigid robot are based on the property of linearity of the equations with respect to a suitable set of dynamic parameters. In general, for a n -DOF manipulator, the dynamic model can be written in the form:

$$\tau = Y(q, \dot{q}, \ddot{q})\delta \quad (4)$$

where δ is a suitable $(p \times 1)$ vector of dynamic parameters and Y is a $(n \times p)$ matrix known as regressor; in our application the torque τ must be set as τ_{PSM} or τ_{MTM} . In principle, vector δ can be obtained by stacking the vectors δ_i of the

dynamic parameters of link L_i , that, in the general case, includes:

- the mass m_i
- the three components of the first moment \mathbf{m}_i ;
- the six independent elements of the inertia tensor \mathbf{I}_i ;
- the static (F_{si}) and viscous (F_{vi}) friction coefficients.

Moreover, in the robots considered here, the link parameters include also:

- the elasticity coefficients K_{ei} for some of the links;
- a constant additive torque $\tau_{o,i}$ modelling the static friction offset, which may also take into account the motor current offset and the residual elastic force of the cables.

Note that the inertia tensor and first moment of link L_i are computed with respect the origin of frame $i - 1$ (frame i) if joint i is revolute (prismatic).

It is known that not all the dynamic parameters of the links appear explicitly in the dynamic model (4) and can be identified. There are some parameters that are unidentifiable due to the mechanical structure of the manipulator and some others that are identifiable only in linear combination [14].

A reduced vector β of $r < p$ parameters can be found using, e.g. a numerical algorithm based on the Singular Value Decomposition (SVD) of the regressor \mathbf{Y} [14], so that:

$$\tau = \mathbf{Y}_r(\mathbf{q}, \dot{\mathbf{q}}, \ddot{\mathbf{q}})\beta, \quad (5)$$

where \mathbf{Y}_r is the $(n \times r)$ reduced regressor. Vector β can be computed as $\beta = \mathbf{K}_I \delta$, where \mathbf{K}_I is a constant $(r \times p)$ matrix of coefficients.

The standard method proposed in the literature to identify the robot dynamic parameters is based on a simple least-squares optimal solution. Namely, if the robot joint torques, as well as the joint positions, velocities and accelerations are measured at given time instants t_1, \dots, t_M along a given trajectory, one may write:

$$\tau_M = \begin{bmatrix} \tau(t_1) \\ \vdots \\ \tau(t_M) \end{bmatrix} = \begin{bmatrix} \mathbf{Y}_r(t_1) \\ \vdots \\ \mathbf{Y}_r(t_M) \end{bmatrix} \beta = \mathbf{Y}_M \beta. \quad (6)$$

The least-squares optimal solution to (6) is obtained through the left pseudo-inverse matrix of \mathbf{Y}_M . More advanced approaches allow to preserve the physical consistency of the parameters [9]. In this work, the method proposed by Sousa e Cortesão [11] is adopted, which is based on a semidefinite programming reformulation of the least squares method.

Since the joint torques of both the PSM and MTM arm may have very different values, numerical errors may occur. These errors can be reduced by multiplying both sides of Eq. (5) by a suitable diagonal weighting matrix $\mathbf{W} = \text{diag}\{w_1, \dots, w_n\}$ whose elements are inversely proportional to the maximum torque measured on the respective joint along a given trajectory, namely: $w_i = 1/\tau_{i,max}$.

Another weighting matrix \mathbf{P} can be introduced to normalise the regressor \mathbf{Y}_M with respect to the difference in magnitude of the parameters, defined as:

$$\mathbf{P} = \text{diag} \left(\frac{1}{\|\mathbf{Y}_{M,1}\|}, \dots, \frac{1}{\|\mathbf{Y}_{M,r}\|} \right), \quad (7)$$

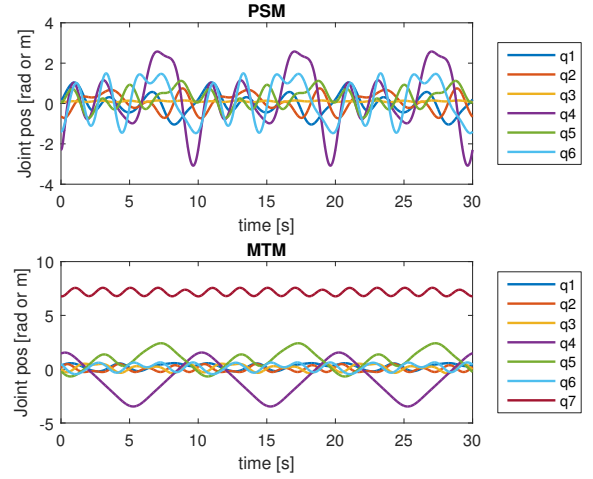


Fig. 5. Identification trajectory for the PSM and the MTM arms

where $\|\mathbf{Y}_{M,i}\|$ is norm of the i -th column of the regressor \mathbf{Y}_M . The optimal solution computed using the weighted regressor $\mathbf{Y}_M \mathbf{P}$ must be multiplied by \mathbf{P}^{-1} to obtain β^* .

IV. OPTIMAL TRAJECTORY GENERATION

The trajectory used for the identification must be sufficiently *rich* to allow an accurate estimation of the dynamic parameters. On the other hand, the trajectory must not excite the unmodeled dynamics, like link or joint elasticity. The condition number of the regression matrix \mathbf{Y}_M is a measure of the sensitivity of the solution $\hat{\beta}$ respect to the errors on \mathbf{Y}_M or τ_M . Therefore the problem of the optimal trajectory generation can be formulated as that of minimising the condition number of the matrix $\mathbf{Y}_M \mathbf{P}$ with \mathbf{P} the weighting matrix defined in (7). The method proposed in [15] is adopted, based on the composition of sinusoidal trajectories for joint i of the form:

$$q_i(t) = \sum_{l=1}^L \frac{a_l^i}{\omega_f l} \sin(\omega_f l t) - \frac{b_l^i}{\omega_f l} \cos(\omega_f l t) + q_{i0} \quad (8)$$

where ω_f is the fundamental frequency and L is the number of the Fourier series harmonics. For both the PSM arm and the MTM arm these parameters have been set to $\omega_f = 0.1$ and $L = 5$. The quantities a_l^i , b_l^i and q_{i0} for $l = 1, \dots, L$ are the degrees of freedom used to minimize the condition number, by solving a nonlinear optimisation problem with $2L + 1$ free variables per joint. It is possible to consider also the constraints deriving from joint positions and velocity limits:

$$\begin{aligned} \mathbf{q}_{\min} &\leq \mathbf{q}(p T_s) \leq \mathbf{q}_{\max} \\ \dot{\mathbf{q}}_{\min} &\leq \dot{\mathbf{q}}(p T_s) \leq \dot{\mathbf{q}}_{\max} \\ \{\mathbf{k}(\mathbf{q}(p T_s))\} &\subset \mathcal{S} \end{aligned}$$

where $p = 0, 1, 2, \dots, T_f/T_s$, T_f is the final time, T_s is the sampling time, \mathcal{S} is the robot workspace and $\mathbf{k}(\mathbf{q})$ is the robot direct kinematic function. The constrained nonlinear optimization method *active-set* included in the function `fmincon` of MATLAB® has been used.

TABLE III

JOINT POSITION AND VELOCITY LIMITS FOR THE PSM

	J1	J2	J3	J4	J5	J6
$q_{min}[deg - m]$	-60	-45	0.05	-180	-90	-90
$q_{max}[deg - m]$	60	45	0.18	180	90	90
$\dot{q}_{min}[rad/s - m/s]$	-2	-2	-0.4	-6	-5	-5
$\dot{q}_{max}[rad/s - m/s]$	2	2	0.4	6	5	5

V. EXPERIMENTAL RESULTS

The optimal identification trajectory computed for the PSM is reported in Fig. 5, with the joint position and velocity limits of Table III. Since the measured currents and joint

TABLE IV

JOINT POSITION AND VELOCITY LIMITS FOR THE MTM

	J1	J2	J3	J4	J5	J6	J7
$q_{min}[deg]$	-40	-15	-50	-200	-90	-45	-480
$q_{max}[deg]$	65	50	35	90	180	45	450
$\dot{q}_{min}[rad/s]$	-1.1	-1.1	-1.1	-2	-2	-2	-2
$\dot{q}_{max}[rad/s]$	1.1	1.1	1.1	2	2	2	2

TABLE V

CARTESIAN SPACE LIMITS FOR THE MTM

	x	y	z
$p_{min}[mm]$	-60	-60	-80
$p_{max}[mm]$	250	100	100

positions are very noisy, all the signals were filtered using a moving average filtering technique. Table VI reports the dynamic parameters of the PSM and their numerical values. Fig. 6 reports the measured torques and those computed

TABLE VI

PSM PARAMETERS

Param	Value	Param	Value	Param	Value
m_{1x}	-0.683	m_{3y}	-0.672	K_{e4}	0.003
F_{v1}	0.133	m_3	0.146	τ_{o4}	0.004
F_{s1}	0.064	m_{3x}	0.033	F_{v55}	0.028
K_{e1}	0.129	m_{3y}	0.001	F_{v56}	0.005
τ_{o1}	0.004	m_{3z}	-0.039	F_{s5}	0.012
F_{v2}	0.136	F_{v3}	2.695	F_{v65}	0.013
F_{s2}	0.15	F_{s3}	0.496	F_{v66}	0.02
K_{e2}	0.35	F_{v4}	0.001	F_{s6}	0.004
τ_{o2}	0.071	F_{s4}	0.004	m_c	0.179

Param	Value
$5I_{2''yz} + 5I_{3yz} + m_{1z} + m_{2z}$	0.013
$I_{2'xx} + I_{2''xx} + I_{3xx} + I_{cxx} + I_{1yy}$ $+ I_{2yy} + 0.04m_{2'} + 0.04m_{2''} - 0.4m_{2''z}$	-0.07
$0.2m_{2'} + 0.2m_{2''} + m_{2x} - m_{2''z}$	-0.091
$m_{2y} - 5I_{3xz} - 5I_{2''xz}$	0.228
$I_{2xx} - I_{2''xx} - I_{3xx} - I_{cxx} - I_{2yy} + I_{2''zz}$ $+ I_{3zz} + I_{czz} - 0.04m_{2'} - 0.04m_{2''} + 0.4m_{2''z}$	0.003
$I_{2''yy} + I_{3yy} + I_{cyy} + I_{2zz} + 0.04m_{2'}$ $+ 0.04m_{2''} - 0.4m_{2''z}$	0.188
$m_{2'z} - 5I_{3yz} - m_{2''y} - 5I_{2''yz}$	-0.022
$5I_{2''xz} + 5I_{3xz} + m_{2''x}$	-0.246
$I_{2''xy} + I_{3xy}$	-0.007

using the dynamic model with the identified parameters, considering a test trajectory different from that used for the identification. The dashed line is the reconstruction error. The corresponding RMS absolute and relative errors are reported in Table VII. The errors are not negligible in particular for the joints 5 and 6, for which only the friction forces have been

TABLE VII

RMS ERRORS ON THE TORQUES FOR THE PSM

	J_1	J_2	J_3	J_4	J_5	J_6
Abs err	0.05	0.08	0.194	0.0010	0.017	0.015
Rel err %	22.07	31.55	29.55	11.93	35.1	45.3

TABLE VIII

RMS ERRORS ON THE TORQUES FOR THE MTM

	J_1	J_2	J_3	J_4	J_5	J_6	J_7
Abs err	0.031	0.097	0.102	0.029	0.011	0.004	0.0005
Rel err %	27.06	21.04	39.07	28.36	43.54	25.42	42.83

considered in the model; however, the results are globally satisfactory considering the high sensors noise, especially on the joint velocities and accelerations, that are computed numerically, and the unmodelled dynamics, like friction and elasticity of the tendons.

TABLE IX

MTM PARAMETERS

Param	Value	Param	Value	Param	Value
F_{v1}	0.129	F_{v3}	0.068	K_{e5}	-0.018
F_{s1}	0.037	F_{s3}	0.0001	τ_{off5}	0.009
K_{e1}	0.249	m_{4x}	0.008	$mpx6$	0.0001
τ_{o1}	-0.032	m_{4z}	-0.034	F_{v6}	0.0001
m_{2y}	0.558	F_{v4}	0.066	F_{s6}	0.005
I_{2xy}	0.008	F_{s4}	0.034	K_{e6}	0.003
F_{v2}	0.119	K_{e4}	0.042	τ_{o6}	-0.002
F_{s2}	0.053	τ_{o4}	0.052	m_{7x}	0.0001
$m_{2'y}$	0.205	m_{5x}	0.002	m_{7y}	0.0001
$m_{2''y}$	-0.541	m_{5y}	-0.053	I_{7zz}	0.0001
$m_{2''z}$	-0.484	F_{v5}	0.0001	F_{v7}	0.001
m_{3y}	-0.014	F_{s5}	0.011	F_{s7}	0.0001

Param	Value
$I_{1yy} + I_{2yy} + I_{2'yy} + I_{2''yy} + I_{3zz} + 0.01m_{2''}$ $+ 0.078m_3 + 0.21(m_4 + m_5 + m_6 + m_7)$	0.217
$0.279m_3 - 0.739(m_4 + m_5 + m_6 + m_7)$ $+ m_{2x} - 2.793m_{3x}$	-0.839
$I_{2xx} + I_{2''xx} - I_{2yy} - I_{2''yy}$ $- 0.078(m_3 + m_4 + m_5 + m_6 + m_7)$	0.029
$I_{2zz} + I_{2''zz} + 0.078(m_3 + m_4 + m_5 + m_6 + m_7)$	0.123
$0.1m_{2''} + 0.36(m_4 + m_5 + m_6 + m_7) + m_{2'x} + m_{3x}$	0.031
$I_{2'xx} + I_{3xx} - I_{2'yy} - I_{3zz} + I_{4zz} - 0.01m_{2''}$ $- 0.13m_4 - 0.11(m_5 + m_6 + m_7)$	-0.588
$I_{3yy} + I_{2'zz} + I_{4zz} + 0.01m_{2''} + 0.13m_4$ $+ 0.15(m_5 + m_6 + m_7)$	0.131
$1.02(m_4 + m_5 + m_6 + m_7) + m_{2''x} + 2.79m_{3x}$	0.951
$0.15(m_5 + m_6 + m_7) + m_{4y} + m_{3z}$	-0.186
$I_{3xz} - 0.055(m_5 + m_6 + m_7) - 0.36m_{4y}$	0.038
$I_{4xx} - I_{4zz} + I_{5zz}$	-0.037
$I_{4yy} + I_{5zz}$	-0.001
$m_{6y} + m_{5z}$	-0.004
$I_{5xx} - I_{5zz} + I_{6zz}$	0.001
$I_{5yy} + I_{6zz}$	0.002

The optimal identification trajectory computed for the MTM is reported in Fig. 5, with the joint position and velocity limits of Table IV. Table V reports the Cartesian space constraints needed to avoid the collision between the MTM arm and the console. Fig. 7 reports the measured and computed torques as for the MTM and the corresponding RMS absolute and relative errors are reported in Table VIII.

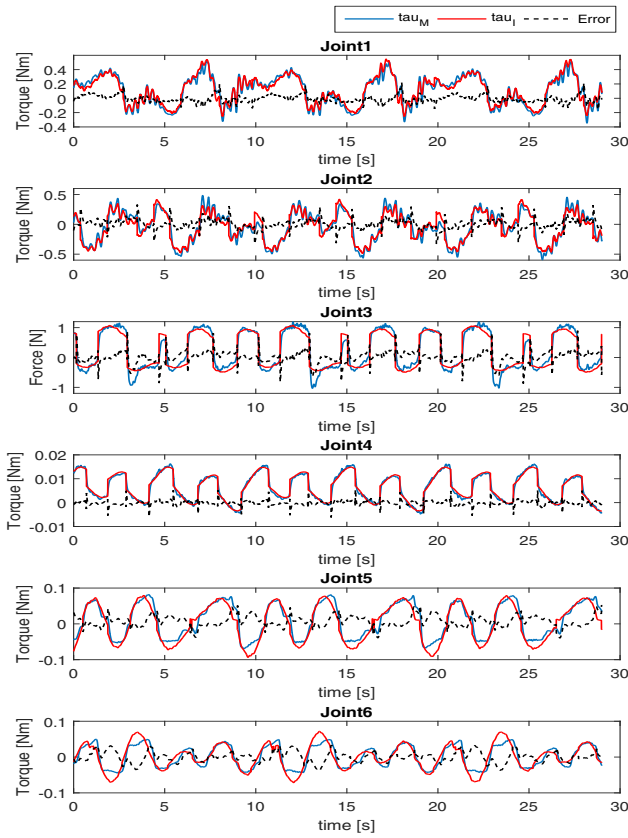


Fig. 6. Measured and computed torques for the PSM along a test trajectory

VI. CONCLUSION AND FUTURE WORKS

In this work the dynamic model identification of the DaVinci Research Kit robotic arms was presented. The minimum number of parameters required to compute the complete dynamic models of the PSM and of the MTM have been derived. An LMI-based constrained approach was used to ensure the physical feasibility of the dynamic parameters and suitable exciting trajectories were derived using an optimality criterion to improve the identification results. The error between the measured torques and those computed using the identified dynamic model remains below 30% for almost all the joints. Future work will be devoted to reduce this error, for example using non-linear friction models for the tendon driven joints, and to test the accuracy of the model-based sensorless estimation of the contact forces.

VII. ACKNOWLEDGMENT

This research has been partially funded by the EC Seventh Framework Programme (FP7) within RoDyMan project 320992 and by the national grant MURH under Programma STAR linea 1.

REFERENCES

- [1] da Vinci Research Kit wiki community. [Online]. Available: <http://research.intusurg.com/dvrkwiki/>
- [2] John Hopkins University DVRK controller git repositories. [Online]. Available: <https://github.com/jhu-dvrk>
- [3] E. Magrini, F. Flacco, and A. D. Luca, "Control of generalized contact motion and force in physical human-robot interaction," in *IEEE Int. Conference on Robotics and Automation*, 2015, pp. 2298–2304.

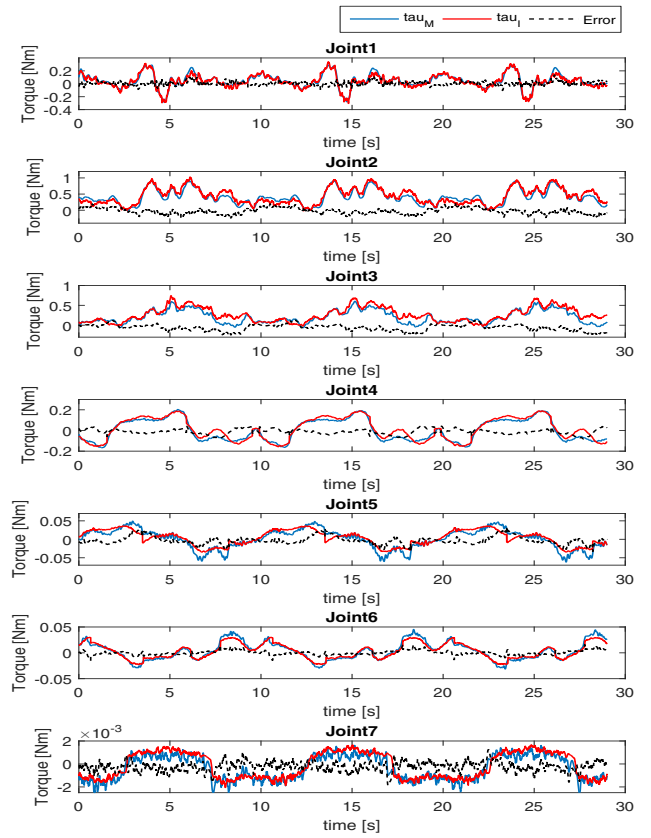


Fig. 7. Measured and computed torques for the MTM along a test trajectory

- [4] A. Cirillo, F. Ficuciello, C. Natale, S. Pirozzi, L. Villani, and B. Siciliano, "A conformable force/tactile skin for physical human-robot interaction," *IEEE Robotics and automation letters*, vol. 1, pp. 41–48, 2015.
- [5] F. Ficuciello, L. Villani, and B. Siciliano, "Variable impedance control of redundant manipulators for intuitive human-robot physical interaction," *IEEE Transactions on Robotics*, vol. 31, pp. 850–863, 2015.
- [6] G. A. Fontanelli, L. Buonocore, F. Ficuciello, L. Villani, and B. Siciliano, "A novel force sensing integrated into the trocar for minimally invasive robotic surgery," in *IEEE/RSJ Int. Conference on Intelligent Robots and Systems*, 2017.
- [7] H. Mayeda, K. Yoshida, and K. Osuka, "Base parameters of manipulator dynamic models," *IEEE Transactions on Robotics and Automation*, vol. 6, pp. 112–128, 1990.
- [8] K. Yoshida and W. Khalil, "Verification of the positive definiteness of the inertial matrix of manipulators using base inertial parameters," *The Int. Journal of Robotics Research*, vol. 19, pp. 498–510, 2000.
- [9] M. Gautier and G. Venture, "Identification of standard dynamic parameters of robots with positive definite inertia matrix," in *2013 IEEE/RSJ Int. Conference on Intelligent Robots and Systems*, 2013, pp. 5815–5820.
- [10] K. Ayusawa and Y. Nakamura, "Identification of standard inertial parameters for large-dof robots considering physical consistency," in *IEEE/RSJ Int. Conference on Intelligent Robots and Systems*, 2010, pp. 6194–6201.
- [11] C. D. Sousa and R. Cortesão, "Physically feasibility of robot base inertial parameters identification: A linear matrix inequality approach," *Int. Journal of Robotics Research*, vol. 33, pp. 931–944, 2014.
- [12] G. Guthart and J. Salisbury, "The intuitiveTM telesurgery system: overview and application," in *IEEE Int. Conference on Robotics and Automation*, 2000, pp. 618–621.
- [13] B. Siciliano, L. Sciacicco, L. Villani, and G. Oriolo, *Robotics*, 2010.
- [14] M. Gautier, "Numerical calculation of the base inertial parameters," in *IEEE Int. Conference on Robotics and Automation*, 1990, pp. 1020–1025.
- [15] J. Swevers, C. Ganseman, D. B. Tükel, and J. De Schutter, "Optimal robot excitation and identification," *IEEE Transactions on Robotics and Automation*, vol. 13, pp. 730–740, 1997.